DES-2019-0438
FERMILAB-PUB-19-621-AE

MNRAS **000**, 000–000 (2018) Preprint 30 January 2020 Compiled using MNRAS LaTeX style file v3.0

arXiv:2001.11015v1 [astro-ph.SR] 29 Jan 2020

Increasing the census of L and T dwarfs in wide binary and multiple systems using Dark Energy Survey DR1 and Gaia DR2 data

M. dal Ponte,[1,2] B. Santiago,[1,2] A. Carnero Rosell,[3,2] B. Burningham,[4] B. Yanny,[5] J. L. Marshall,[6] K. Bechtol,[7,8] P. Martini,[9,10] T. S. Li,[11,5,12,13] L. De Paris,[1] T. M. C. Abbott,[14] M. Aguena,[15,2] S. Allam,[5] S. Avila,[16] E. Bertin,[17,18] S. Bhargava,[19] D. Brooks,[20] E. Buckley-Geer,[5] M. Carrasco Kind,[21,22] J. Carretero,[23] L. N. da Costa,[2,24] J. De Vicente,[3] H. T. Diehl,[5] P. Doel,[20] T. F. Eifler,[25,26] S. Everett,[27] B. Flaugher,[5] P. Fosalba,[28,29] J. Frieman,[5,12] J. García-Bellido,[16] E. Gaztanaga,[28,29] D. W. Gerdes,[30,31] D. Gruen,[32,12,33] R. A. Gruendl,[21,22] J. Gschwend,[2,24] G. Gutierrez,[5] S. R. Hinton,[32] D. L. Hollowood,[27] K. Honscheid,[9,35] D. J. James,[36] K. Kuehn,[37,38] N. Kuropatkin,[5] M. A. G. Maia,[2,24] M. March,[39] F. Menanteau,[21,22] R. Miquel,[40,23] A. Palmese,[5,12] F. Paz-Chinchón,[21,22] A. A. Plazas,[11] E. Sanchez,[3] V. Scarpine,[5] S. Serrano,[28,29] I. Sevilla-Noarbe,[3] M. Smith,[41] E. Suchyta,[42] M. E. C. Swanson,[22] G. Tarle,[31] D. Thomas,[43] T. N. Varga,[44,45] and A. R. Walker [14]

(DES Collaboration)

Affiliations are listed at the end of the paper.

Accepted XXX. Received YYY; in original form ZZZ

ABSTRACT

We present the discovery of 255 binary and six multiple system candidates with wide (> 5") separation composed by L or T dwarfs companions to stars, plus nine double brown dwarf systems. The sample of brown dwarf candidates was found in the Dark Energy Survey and the possible stellar companions are from Gaia DR2 and DES data. Our search is based in a common distance criterion with no proper motion information. For the Gaia DR2 stars we estimate distances based on their parallaxes and photometry, using the `StarHorse` code, while for DES stars, the `StarHorse` distances were purely photometric for the majority of cases, with a fraction having parallax measurement from Gaia DR2. L and T dwarfs distances are based on empirical templates ranging from L0 to T9. We also compute chance alignment probabilities in order to assess the physical nature of each pair. We find 174 possible pairs with Gaia DR2 primaries with chance alignment probabilities < 5%. We also find 85 binary pair candidates with a DES star as a primary, 81 of them with chance alignment probabilities < 5%. Only nine candidate systems composed of two brown dwarfs were identified. The sample of multiple systems is made up of five triple systems and one quadruple system. We determine that the typical wide binary fraction over the L and T spectral types is 2 − 4%. The significant leap provided by this sample will enable constraints on the formation and evolution of L and T dwarfs.

Key words: binaries: general - brown dwarfs - surveys

1 INTRODUCTION

L,T and Y dwarfs, also called brown dwarfs, are presumed to be common objects in the Milky Way. Due to their very low masses ($< 0.075 M_\odot$) and temperatures ($T_{\rm eff} < 2300K$), and hence luminosities, they are difficult sources to detect.

The census of brown dwarfs has greatly improved since the appearance of infrared surveys, such as the Two-Micron All-Sky Survey (2MASS; Skrutskie et al. 2006), the Deep Near Infrared Survey of the Southern Sky (DENIS; Epchtein et al. 1997), the UKIRT Infrared Deep Sky Survey (UKIDSS; Lawrence et al. 2007), the Wide-field Infrared Survey Ex-

© 2018 The Authors

plorer (WISE; Wright et al. 2010) and the VISTA Hemisphere Survey (VHS; McMahon et al. 2013). Among the optical surveys that unveiled substantial numbers of such cool sources are the Sloan Digital Sky Survey (SDSS; York et al. 2000), and, more recently, the Dark Energy Survey (DES; Abbott et al. 2018). However, samples of known brown dwarfs are still restricted to distances of a few hundred parsecs from the Solar position.

On the theoretical side, many uncertainties about the interior, atmosphere and evolution of L and T dwarfs still remain. Models of brown dwarf structure often lack consistent boundary conditions between the interior and the atmosphere. Uncertainties also remain in terms of opacities, the equation of state and the importance of cloud condensation in the atmospheres (Pinfield et al. 2012). As in the case of stars, brown dwarf formation and evolution models should benefit from knowledge of chemical composition, masses and ages of a sizeable sample of such objects. Binary systems are ideal for this purpose since the physical properties of the primary star can be applied to the brown dwarf companion, assuming that the pair formed at the same time, of the same material and evolved in the same environment (Faherty et al. 2010). Also, large statistical samples could constrain the behavior and intrinsic variations of formation and properties of the L and T dwarf population.

In terms of binary statistics, there is evidence that the binary frequency decreases as a function of spectral type and separation. For solar-type stars, Raghavan et al. (2010) found that ~ 25% have a companion with separation wider than 100 astronomical units (AU), ~ 11 % wider than 1,000 AU and Tokovinin & Lépine (2012) estimate 4.4 % wider than 2,000 AU. However, searches for M, L or T dwarfs in wide binary systems remains incomplete. Recently Dhital et al. (2011) and Dhital et al. (2015) presented the Sloan Low-mass Wide Pairs of Kinematically Equivalent Stars (SLoWPoKES), a catalogue containing common proper motion and common distance wide candidate pairs. For the mid-K and mid-M type dwarfs presented in both catalogues, the wide binary frequency was ~ 1.1%. However, the binary fraction for L and T dwarfs in wide systems is still uncertain. The fraction of L and T dwarfs found in binary and multiple systems, the distributions of mass ratios, primary spectral types, and separations may constrain different scenarios to the different scenarios proposed for the formation of brown dwarfs (Bonnell et al. 2008; Bate & Bonnell 2005; Whitworth & Zinnecker 2004; Elmegreen 2011).

Using DES, VHS and WISE data we were recently able to select and perform spectral classification using only photometry on a sample of 11,745 brown dwarf candidates (Carnero Rosell et al. 2019). Using this sample of L and T dwarfs we estimated the thin disk scale height of L dwarfs (~ 450 pc), which agreed with a recent measurement by Sorahana et al. (2018). A more detailed description of the data, colour cuts, spectral classification and modeling of the spatial distribution of L and T dwarfs is presented in Carnero Rosell et al. (2019).

In this paper we present the search of benchmark systems, specifically wide binary or multiple systems which contain L and T dwarf companions. These systems are useful to improve brown dwarf evolutionary models since their chemical composition and age constraints may be taken from the primary star, since those physical properties are difficult to measure for brown dwarfs. Estimates of the fraction of L and T dwarfs in multiple systems may also constrain their main formation scenarios. In Section 2 we describe the catalogues used in our work and the selection criteria used to select samples of stars and brown dwarfs from them. In Section 3 we briefly describe our sample of brown dwarf candidates selected using DES, VHS and AllWISE data. In Section 4 we discuss the photometric distance measurement for the L and T candidates and the spectrophotometric distance for the primary stars selected in the Gaia DR2 and DES data. In Section 5 we present the the properties of candidate binaries and also we address the estimation of chance alignment probability.

2 CANDIDATE SELECTION OF BROWN DWARFS AND PRIMARY STARS

2.1 DES, VHS and WISE data

DES is a (~5,000deg^2) optical survey in the $grizY$ bands used the Dark Energy Camera (DECam; Flaugher et al. 2015). DECam is a wide-field (3 deg^2) imager at the prime focus of the Blanco 4m telescope in Cerro Tololo Inter-American Observatory (CTIO).

The DES footprint was selected to obtain a overlap with the South Pole Telescope survey (Carlstrom et al. 2011) and Stripe 82 from SDSS (Abazajian et al. 2009). The Galactic plane was avoided to minimize stellar foregrounds and extinction from interstellar dust in order to maintain the DES cosmological goals. Even though the main drive for DES is cosmological, the stellar data have been extensively used by the collaboration to identify new star clusters, streams and satellite galaxies in the MW Halo and beyond (Bechtol et al. 2015; Drlica-Wagner et al. 2015; Luque et al. 2017).

The first public data release of the Dark Energy Survey, DES DR1 (DR1; Abbott et al. 2018) is composed of 345 distinct nights spread over the first 3 years of DES operations, from 2013 August 15 to 2016 February 12. The DES DR1 catalogue contains object flags including several that indicate corrupted values due to image artifacts or reduction problems. For the searches of L and T dwarfs and the primary stars in the DES data, we demanded that `FLAGS_z,Y` = 0 (ensures no reduction problems in the z and Y bands) and `ISO_MAGFLAGS_i,z,Y` = 0 (ensures the object has not been affected by spurious events in the images in i,z,Y bands). In the more specific case of the brown dwarfs search, we also imposed a magnitude limit cut of $z < 22$ with a detection of 5σ at least in the z and Y to ensure a high completeness in the i band. For the primary stars case, we imposed a magnitude limit cut of $i < 24$. The DES DR1 is a already a public release, but in this work we used `SOF_PSF_MAG_i,z` photometry, which has not been published yet. The SOF photometry is based on a different reduction using the `ngmix` code [1], which has better PSF and shape modeling. Even though we used nonpublic photometry, the `COADD_ID` are the same as those in the public release.

In order to obtain more photometric bands, we also used VHS and AllWISE data and matched them to the DES DR1 data. The infrared magnitudes were used in the photometric

[1] https://github.com/esheldon/ngmix

distance estimation, as we will present in detail in Section 4.2. We first matched DES to VHS using a positional matching radius of 2”, and then we repeated the same procedure with the AllWISE catalogue using the resulting DES and VHS catalogue. After matching the DES, VHS and AllWISE data, we removed every source that did not pass the DES quality cuts as explained before. The resulting catalogues have 27,249,118 and 27,918,863 sources within a 2374 deg^2 overlap region. These two catalogues were used for the L and T dwarf search (Section 3) and to search for primary star candidates (Section 5.2), respectively.

2.2 Gaia

The Gaia astrometric mission was launched in December 2013. It is measuring positions, parallaxes, proper motions and photometry for over one billion sources to $G \simeq 20.7$. Its Data Release 2 (Gaia DR2; Gaia Collaboration et al. 2018), has covered the initial 22 months of data taking (from a predicted total of 5 years), with positions and photometry for 1.7×10^9 sources and full astrometric solution for 1.3×10^9.

For our purpose, we used Gaia DR2 data to select primary star candidates. Particularly important for this work are the parallaxes, whose precision varies from < 0.1 mas for $G \leq 17$ to $\simeq 0.7$ mas for $G = 20$. They allow us to better discern dwarfs (whose distances will overlap those of the brown dwarfs from DES, VHS and AllWISE) from much more distant giants of similar colours, $T_{\rm eff}$ and chemistry. For the stars brighter than G=18, the Gaia DR2 sample was cross-matched to the Pan-STARRS1 (Kaiser et al. 2010), 2MASS and AllWISE catalogues, so as to increase the amount of photometric information available for each star as we did for DES. The derived photo-astrometric distances are presented in Anders et al. (2019).

3 SAMPLE OF L AND T CANDIDATES

The search of L and T dwarf candidates in the combination of DES, VHS and AllWISE data was performed using a colour-colour cut criteria. We adopted $(i_{AB} - z_{AB}) > 1.2$, $(z_{AB} - Y_{AB}) > 0.15$ and $(Y_{AB} - J_{Vega}) > 1.6$ to select our candidates.

We used this initial sample, mainly made up of M, L and T dwarfs, to run our spectral classification code, *classif*, which uses only photometry, to estimate the spectral type of each object of the sample. The *classif* code was implemented using the same method presented in Skrzypek et al. (2015) and Skrzypek et al. (2016), based on a minimization of the χ^2 relative to M, L and T empirical templates. We also ran `Lephare` photo-z code (Arnouts et al. 1999; Ilbert et al. 2006) to access the possible extragalactic contamination. After running *classif* and `Lephare` we obtained 2,818 sources classified as galaxies or quasars, 20,863 classified as M, and 11,545 classified as L dwarfs and 200 as T dwarfs. More details about the selection method and the spectral classification can be found in Carnero Rosell et al. (2019).

4 DISTANCE MEASUREMENT

4.1 L and T dwarf candidates

Using our L and T sample described in Section 3, we used the spectral type from each candidate and our empirical model grid described in Carnero Rosell et al. (2019) to estimate the absolute magnitude and then obtain the distance modulus for each L and T dwarf.

The empirical model grid lists absolute magnitudes in $izYJHKW1W2$ for dwarfs ranging from M1 to T9. We computed one distance modulus for each filter with available apparent magnitude. The resulting distance to each L and T dwarfs was then taken to be the mean value among the available filters and we used the dispersion around the mean as the distance uncertainty. We did not apply any correction for extinction, since this is expected to be small for the passbands we used and towards the relatively high Galactic latitudes covered by our samples.

4.2 Primary stars

As mentioned before, we use the Gaia DR2 (Gaia Collaboration et al. 2018) and the combination of DES, VHS and AllWISE to search for stars located close to our L or T dwarf candidates. Anders et al. (2019) ran the `StarHorse` code (Queiroz et al. 2018) on all stars in the Gaia DR2 sample brighter than $G = 18$, in an attempt to better constrain their distances and extinction. For DES stars, `StarHorse` was applied by us, but only to the stars that were close enough to the L or T candidates to be considered as a potential companion, as will be discussed in the next section. In this latter case, we use optical and infrared photometry, in addition to parallaxes from Gaia DR2 when available.

The `StarHorse` code uses a Bayesian approach to determine masses, ages, distances and extinctions for field stars through the comparison of their observed spectroscopic, photometric and astrometric parameters with those from stellar evolution models. The models used were materialized by the `PARSEC` set of isochrones (Bressan et al. 2012). The code assumes spatial priors for each structural component of the Galaxy (thin and thick disks, bulge and halo). The priors also assume Gaussian metallicity and age distribution functions for each structural component. For all components, the Chabrier Initial Mass Function (IMF; Chabrier 2003) was assumed as a prior. Gaussian likelihood functions were generated using the available observed parameter set and their associated uncertainties. The code then computes the posterior distribution function over distance, marginalized for all other parameters. We take the median of this marginalized posterior as the best distance estimate, while the difference between the median 84th percentile and the (16th percentile) distances is taken as the higher (lower) 1-σ uncertainty. For more details we refer to Queiroz et al. (2018) and Anders et al. (2019).

5 THE SEARCH FOR BENCHMARK CANDIDATES

Detection of faint sources close to brighter stars is difficult, with detections pushed to larger separations as the difference in brightness increases. We paired L and T candidates

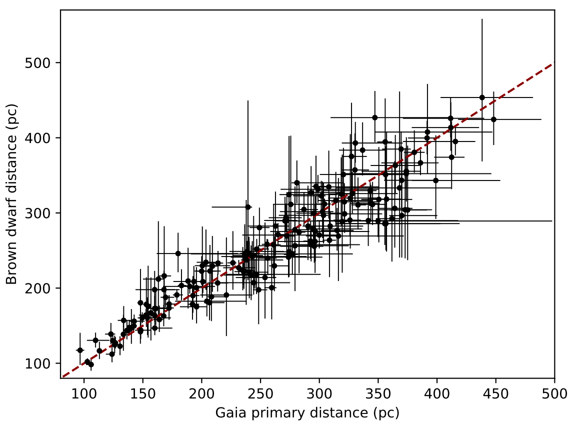

Figure 1. The 174 common distance pair candidates identified using the brown dwarf sample and Gaia DR2 primary candidate stars. The horizontal axis represents the primary distance given by StarHorse and the vertical axis shows the secondary's photometric distance. The error bars correspond to an uncertainty of 2σ. The uncertainties in the photometric distances of the brown dwarf sample are usually much larger than those of the Gaia stars, which are based on measured parallaxes.

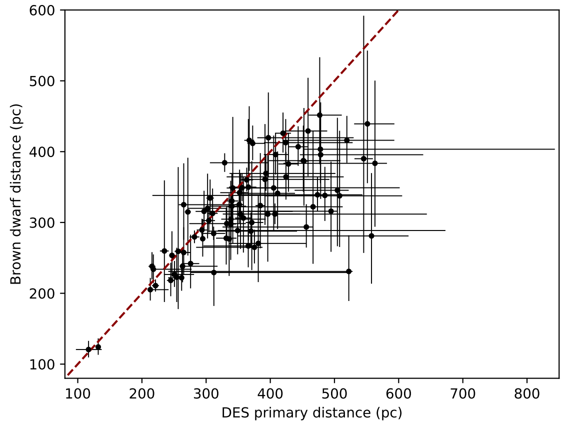

Figure 2. The 85 common-distance pair candidates identified using the brown dwarf sample and DES primary candidate stars. The horizontal axis represents the primary photometric distance given by StarHorse and the vertical axis shows the brown dwarf photometric distance. The error bars indicates an uncertainty of 2σ.

to potential primary stars using a search radius that corresponds to 10,000 AU as the projected distance between the pair members. Since the distances of our L/T candidates are in the [50, 500] pc range, these search radii cover the angular range from 20" to 200". Details on how this projected distance is computed vary with the sample of primaries, as discussed in the next subsections. As discussed in Marocco et al. (2017) and Deacon et al. (2014), searches beyond 10,000 AU also introduce a significant difficulty of disentangling widest binaries from chance alignments from field stars. In the following sections, we describe how the pairing was done for each set, and also discuss the way chance alignment probabilities were computed in each case.

5.1 Brown dwarfs companions to Gaia DR2 stars

For the Gaia DR2 primary candidate stars, we considered their `StarHorse` distances and the photometric distances to the L and T candidates. We defined a search radius equal to a projected separation of 10,000 AU at the lower limit in distance of the Gaia star, given its smaller uncertainty as compared to the brown dwarf. For each star, we then searched for possible L or T companions within this radius. In order to refine our analysis, we also demanded that the distances of the primary and the secondary are within 2σ of each other. Using this common distance criteria, we found 174 candidate pairs as shown in Figure 1. The properties for a subset of these candidate pairs are presented in Table 1. The entire table is available in machine-readable format in `https://des.ncsa.illinois.edu/releases/other/y3-lt-widebinaries`.

For each possible pair, we first estimate the chance alignment probability following an similar procedure used by Smart et al. (2017) and Dhital et al. (2015). The chance alignment probability is the probability that we find a physically unrelated object with the same common distance within our uncertainties. Our search is based only in common distance and does not include any kinematic criteria. Therefore the probability of chance alignment could be high.

To assess the chance alignment probability, we simulate stars within a 2 deg^2 area from the L or T candidate using `Trilegal` (Girardi et al. 2005). The `Trilegal` simulated stars have a distance modulus without any uncertainty. In order to mimic an uncertainty in their distances, we use the uncertainty computed by `StarHorse` for the Gaia DR2 star whose distance is closest to that of the simulated `Trilegal` star. We thus assume that the uncertainty in distance for the simulated stars follows the same distribution as computed by `StarHorse` for real stars. We randomly selected half of the stars within the 2 deg^2 area and demanded that the distances of brown dwarf and the random star were within 2σ of each other. We calculate the fraction N/M of such common distance stars, where N is the number of stars which have the common distance with the L or T candidate and M is the total number of randomly selected stars. Then we obtain the probability over all stars within the search radius by making an area normalization considering the search radius area and the simulated area. We flag every pair with a chance alignment probability $P_a > 5\%$ as possible contamination. In the case of the 174 wide binary pairs identified with Gaia DR2, all of them have $P_a < 5\%$.

Table 1. The common-distance pair candidates identified using the brown dwarf sample, Gaia DR2 and DES DR1 data. The ID in $Jhhmm \pm ddmm$ format using the primary coordinates. The ID with a * symbol indicates that the distance for Gaia DR2 stars was published by Anders et al. (2019). The letter A represents the primary star and B the secondary. The angular and the projected separation are indicated by $\Delta\theta$ and d_P, respectively. The P_a refers to the chance alignment probability, as explained in Section 5.1 and 5.2.

ID	Position				Photometry				Distance		Sp. Type	Binary Information		
	α_A	δ_A	α_B	δ_B	$G_{Gaia,A}$	$z_{DES,A}$	$i_{DES,B}$	$z_{DES,B}$	d_A	d_B	B	$\Delta\theta$ (")	d_P (AU)	P_a (%)
J0001−4315*	00:01:52	-43:15:45	00:01:51	-43:15:41	17.2	15.9	23.0	21.4	295±24	279±15	L1	15.0	4427.4	0.212
J0002+0006*	00:02:10	+00:06:28	00:02:08	+00:07:06	15.4	14.1	22.0	20.4	172±5	179±10	L1	43.1	7440.3	0.217
J0002−0626*	00:02:24	-06:26:11	00:02:23	-06:26:30	16.7	15.2	20.6	19.1	130±2	123±12	L0	34.3	4482.0	0.466
J0003−5803*	00:03:24	-58:03:51	00:03:18	-58:04:06	14.1	12.8	21.2	19.9	154±1	175±48	L0	50.3	7776.1	1.165
J0005+0104	00:05:46	+01:04:54	00:05:47	+01:04:43	18.8	17.2	23.0	21.5	393±82	369±25	L0	14.1	5580.9	0.960
J0008−4929*	00:08:07	-49:29:27	00:08:08	-49:29:20	17.7	16.4	22.6	21.3	314±23	316±36	L0	16.0	5054.3	0.665
J0008−0437	00:08:15	-04:37:53	00:08:17	-04:37:38	18.1	16.7	22.4	20.8	375±52	265±24	L0	26.6	10017.4	0.984
J0009−0109*	00:09:48	-01:09:00	00:09:49	-01:08:10	16.7	15.1	22.2	20.7	190±22	202±10	L1	52.7	10015.1	0.248

Table 2. The nine common distance pair candidates identified among the brown dwarf sample. The ID in $Jhhmm \pm ddmm$ format using the primary coordinates. The letters A and B represent a different brown dwarf. The angular and the projected separation are indicated by $\Delta\theta$ and d_P, respectively. The P_a refers to the chance alignment probability.

ID	Position				Photometry				Distance		Sp. Type		Binary Information		
	α_A	δ_A	α_B	δ_B	$i_{DES,A}$	$z_{DES,A}$	$i_{DES,B}$	$z_{DES,B}$	d_A	d_B	A	B	$\Delta\theta$ (")	d_P (AU)	P_a (%)
J0003−0011	00:03:30	-00:11:06	00:03:35	-00:12:59	23.1	21.0	20.6	19.1	70 ±15	75 ±5	L7	L2	131.5	9141.83	0.078
J0443−4551	04:43:10	-45:51:55	04:43:04	-45:50:23	25.0	21.9	-	21.7	57 ±8	44 ±6	T5	T6	112.0	6345.85	0.020
J0457−4933	04:57:49	-49:33:56	04:57:52	-49:34:02	22.6	21.1	22.4	20.9	304±30	287±38	L0	L0	25.61	7777.43	0.007
J2000−5342	20:00:12	-53:42:38	20:00:12	-53:43:07	23.1	21.3	22.3	20.9	234±54	274±33	L2	L0	29.41	6857.05	0.115
J2251−4959	22:51:57	-49:59:32	22:51:56	-50:00:01	22.9	21.4	23.0	21.4	372±59	349±44	L0	L0	29.51	10961.6	0.170
J2313−4550	23:13:49	-45:50:29	23:13:49	-45:50:25	22.2	20.3	23.3	21.2	87 ±16	114±16	L4	L5	4.080	352.297	0.000
J2318−5420	23:18:39	-54:20:34	23:19:03	-54:21:49	18.4	17.0	21.4	19.9	47 ±3	54 ±9	L0	L5	226.4	10514.6	0.025
J2319−5203	23:19:43	-52:03:55	23:19:48	-52:04:24	21.4	19.9	21.4	19.9	177±10	181±15	L0	L0	59.10	10411.8	0.045
J2319−5607	23:19:50	-56:07:27	23:19:47	-56:07:56	22.1	20.6	22.4	21.0	184±35	225±30	L1	L1	37.21	6832.95	0.066

Table 3. The common-distance multiple systems found in our search. The letter A and B represents a star from Gaia DR2 or DES DR1 and C the brown dwarf. In the last row, the B and C represents a different brown dwarf. The ID in $Jhhmm \pm ddmm$ format using the primary coordinates. The ID with a * symbol indicates that the distance for Gaia DR2 stars was published by Anders et al. (2019). The P_a refers to the chance alignment probability.

ID	Position						Photometry			Distance			Sp. Type		Binary Information
	α_A	δ_A	α_B	δ_B	α_C	δ_C	$G_{Gaia,A}$	$G_{Gaia,B}$	$z_{DES,C}$	d_A	d_B	d_C	B	C	P_a(%)
J0009−5313*	00:09:06	-53:13:30	00:09:06	-53:13:34	00:09:03	-53:13:43	16.8	17.0	23.0	241±5	231±6	235±35		L2	0.371
J0042−0331*	00:42:33	-03:31:29	00:42:33	-03:31:30	00:42:34	-03:31:53	17.9	16.4	21.7	200±18	193±12	194±33		L0	0.481
J0239−0512*	02:39:43	-05:12:59	02:39:44	-05:12:54	02:39:45	-05:13:17	17.0	20.6	20.9	355±44	345±16	286±30		L0	0.471
J2024−5801*	20:24:13	-58:01:15	20:24:14	-58:01:15	20:24:16	-58:01:15	16.9	16.2	22.3	231±9	222±8	218±14		L1	0.228
J2200−4155*	22:00:25	-41:55:02	22:00:25	-41:55:02	22:00:25	-41:55:37	17.3	17.3	20.9	198±12	202±12	214±6		L1	0.024
J2342−6135	23:42:06	-61:35:44	23:42:08	-61:35:42	23:42:04	-61:35:17	20.2	-	20.7	267±36	286±59	279±59	L0	L0	1.360

5.2 Brown dwarfs companions to DES DR1 stars

We also search for primary stars using the combined DES, VHS and AllWISE data. In this case, the search radius corresponds to 10,000 AU projected separation evaluated at the lower distance limit for the L or T dwarf. We adopt this threshold because we do not have the `StarHorse` distances for the entire DES stars catalogue. Due to computational restrictions, we only obtain the `StarHorse` distance for stars that were inside the brown dwarf search radius. Considering that the brown dwarfs do have a large uncertainty in their purely photometric distances, this conservative approach should result in a larger search radius and the inclusion of several stars within this radius.

As mentioned in the previous section, in this case `StarHorse` distances were based on photometric measurements, with additional constraint from parallaxes for a small number of DES primary stars which are common to Gaia DR2. We thus look for pairs within the search radius of each L or T candidate which also have a distance match within 2σ. Using the DES DR1 data we found a total of 85 possible pairs involving a DES DR1 primary and an L or T as a secondary, as shown the Figure 2.

As we explain in the previous section, for the chance alignment probabilities, we rely on `Trilegal` simulations. The procedure is the same as described in Section 5.1. We assign distance uncertainties to the simulated stars using the closest DES DR1 star and then require that the distances of the brown dwarf candidate and the simulated star lie within 2σ of each other. Then we obtain the probability over all stars within the search radius. Also, for DES stars, we randomly selected 5,000 stars to obtain the chance alignment probability since all the simulated areas have more than 10,000 stars. In the case of the 85 wide binary pairs identified with DES DR1, 81 pair candidates have $P_a < 5\%$. The properties for a subset of these candidate pairs are presented in Table 1. The entire table is available in `https://des.ncsa.illinois.edu/releases/other/y3-lt-widebinaries`.

5.3 Multiple systems

In addition to our wide binary pairs presented in Section 5.1 and Section 5.2, we find several candidate multiple systems: five triple and one quadruple system. The quadruple system is composed of three stars associated with a brown dwarf. One of the triple systems is composed by two brown dwarfs and a star. The multiple systems are shown in Figure 3 and their main characteristics are described in Table 3. For more details regarding the table content visit `https://des.ncsa.illinois.edu/releases/other/y3-lt-widebinaries`.

For the multiple systems, the chance alignment probability were computed as explained in Section 5.1 and Section 5.2. We compute the probability considering pairs, e.g. a brown dwarf companion to a star. In the case of higher order systems, we multiply the probability found considering the pairs (BD+star) that the system can constitute. The P_a are shown in the last column of Table 3.

6 WIDE BINARIES INVOLVING TWO BROWN DWARFS

We also used the L and T candidates sample to search for binaries among themselves. We computed a search radius for each L or T dwarf and checked if another brown dwarf appears inside this individual radius. We were able to identify nine possible pairs, which are shown in Figure 4. The properties of these possible binary pairs are presented in Table 2. All nine pairs are matched independently of the pair member that we centered on. In other words, if source B is found within the search radius of 10,000 AU around source A, this latter was also within the same projected separation at B's distance, in all cases.

To obtain the chance alignment probability we used the `GalmodBD` simulation code, presented in Carnero Rosell et al. (2019), which computes expected Galactic counts of L and T dwarfs as a function of magnitude, colour and direction on the sky. `GalmodBD` also creates synthetic samples of brown dwarfs based on the expected number counts for a given footprint, using empirically determined space densities of objects, absolute magnitudes and colours as a function of spectral type. For the current purpose, we computed the expected number of L and T dwarfs in a given direction and within the volume bracketed by the common range of distances and by the area within the angular separation of each possible pair. In all cases, the probability of chance alignment is $P_a < 0.2$ %, as shown in Table 2. For more details regarding the table content visit `https://des.ncsa.illinois.edu/releases/other/y3-lt-widebinaries`.

7 DISCUSSION

For our 264 pair candidates, we visually inspected the DES images. Figure 5 shows a sample of some selected binary candidates considering the pairs constituted by a brown dwarf companion to a Gaia DR2 and DES DR1 star and also systems made up by two brown dwarfs. All of the images were taken from the DES Science Portal related to the DR1 public release images [2].

Figure 6 shows the spectral type of the brown dwarfs versus the projected separation of the pairs. Our sample of wide binary pairs contains 271 L dwarfs companions to stars with projected separations ranging from > 400 AU to 24,000 AU. Only one double T dwarf system was found, with a projected separation > 6,000 AU. Deacon et al. (2014) pointed out the paucity of T dwarfs companions wider than 3,000 AU, which means that this system may be a rare find.

Figure 7 shows the projected separation versus the heliocentric distance of our candidates. Our brown dwarf sample is limited to ~ 480 pc and, despite our previous projected separation limit of 10,000 AU, we end up having some pairs with a value larger than that limit. The reason is due to how we obtained our search radius. We computed a radius value that corresponds to 10,000 AU projected separation at the lower limit distance of each star or brown dwarf. We decided to use the lower distance to increase the search radius. In many cases, this approach will translate into a larger projected separation compared to our initial limit. However,

[2] `https://des.ncsa.illinois.edu/releases/dr1/dr1-access`

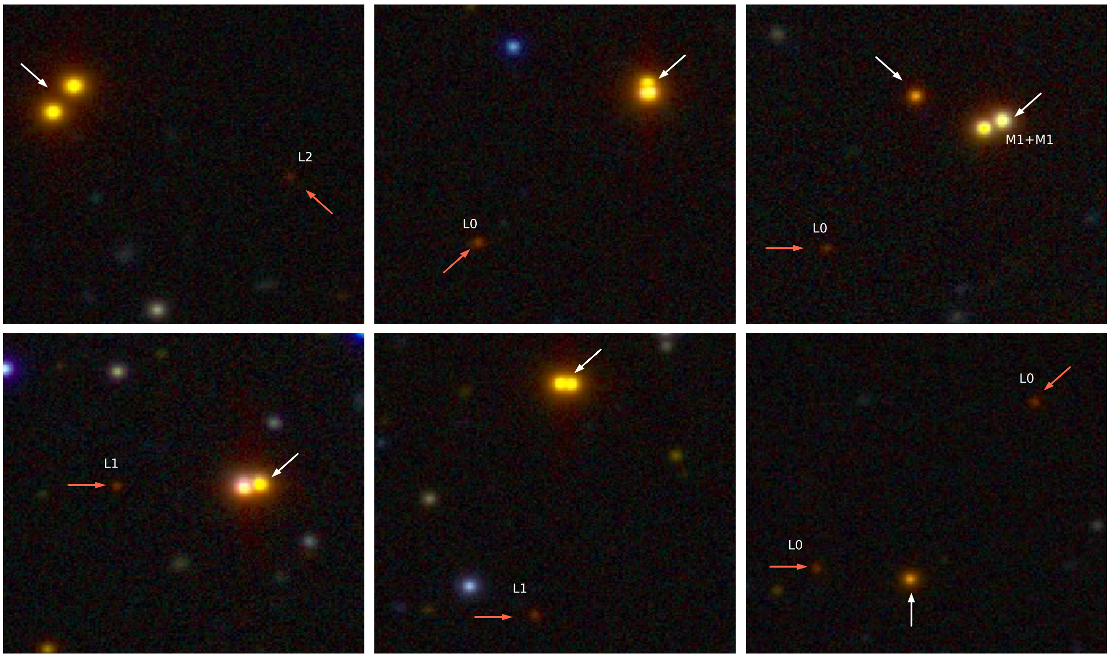

Figure 3. 40"×40"$grizY$ composite images of the multiple systems found. The white arrow indicates the stars, while the brown dwarfs are identified by a red arrow followed by their spectral type. The upper right image corresponds to a quadruple candidate system. The double M1+M1 were previously identified by Dhital et al. (2015). This quadruple system also contains a common distance L0 and a DES star, indicated by the arrows. The remaining images correspond to candidates of triple systems. The lower right panel corresponds to two brown dwarf companions to a DES star.

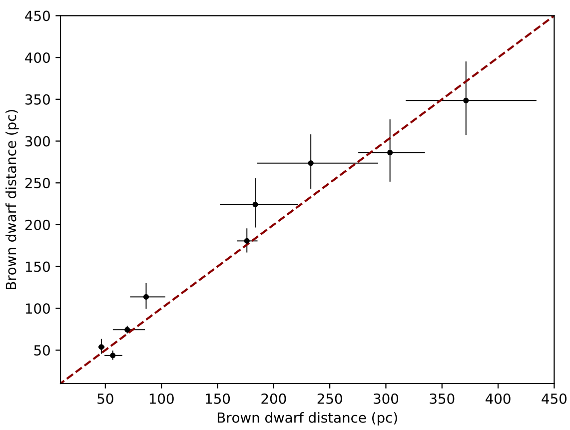

Figure 4. The nine common distances for the pure brown dwarf binary candidates identified. The horizontal and vertical axis show the brown dwarfs photometric distances and the error bars correspond to an uncertainty of 2σ.

82% of our pair candidates concentrate at a distance >400 pc and projected separation < 10,000 AU as illustrated in Figure 7. Also, for the brown dwarfs companions to DES DR1 or Gaia DR2 stars, we notice that the chance alignment probability grows with the projected separation and heliocentric distance of the primary.

Figure 7 also shows a lower limit in projected separation which is related to the typical angular resolution of the DES DR1 and Gaia DR2 images, especially the former, from which the brown dwarf sample is drawn. Pairs whose angular separation is of the order or lower than the DES seeing limit will be harder to resolve. At a distance of 480 pc, a 1.3 arcsec resolution limit will translate into a minimum separation of $\simeq$ 620 AU, which is roughly what Figure 7 shows as a lower limit.

The left panel of Figure 8 shows the frequency distribution of L and T spectral types both in our total sample of brown dwarfs and for the wide binary systems. In both samples, the L0 dwarfs dominate. Even in a deep optical survey such as DES, we are still bound to detect mainly L types at $\sim$ 500 pc and this selection bias against later types clearly appears in the distributions. The right panel shows the fraction of wide binaries (within the projected separation limits discussed earlier) as a function of spectral type. We observe that the typical wide binary fraction is 2-4% over most of the spectral types.

In Table A1 we present the known F/G/K/M+L or T wide pairs already published in the literature that were spectroscopically confirmed and have a brown dwarfs as a companion. In Table A2 we present the common distance and/or common proper motion known F/G/K/M+L or T wide pairs identified so far. Using this information, we searched for matches between our pairs and multiple system candidates presented in this work and the previously known pairs, but neither of the 264 pairs and six multiples were identified among them. The main reason is that the majority of the know wide binaries with spectroscopic confirmation are in the northern hemisphere and/or have a projected separation < 600 AU and we are not able to resolve them.

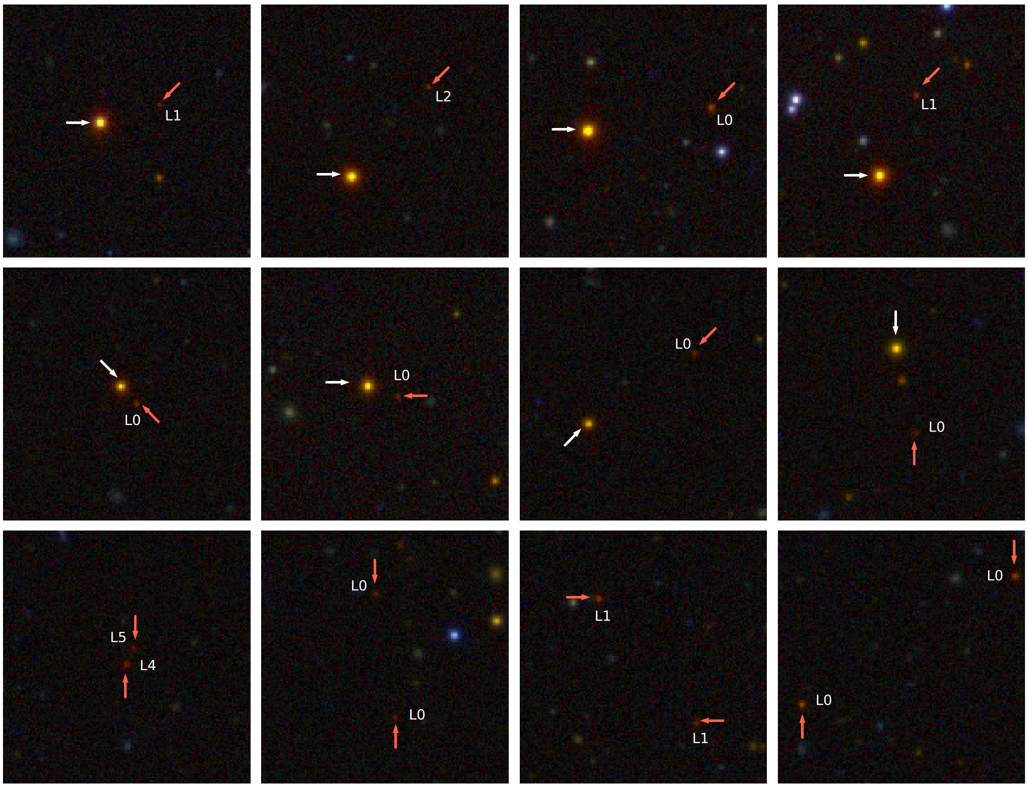

Figure 5. 50" $\times$ 50"$grizY$ composite images of selected binary candidates systems. In the first row, we present L dwarfs as companions of Gaia DR2 stars. In the second row, the L dwarfs as companions of DES stars. In the last row, we present binary pairs composed by two brown dwarfs. In all images the primary star is identified by an white arrow and the brown dwarf by a red arrow followed by their spectral type.

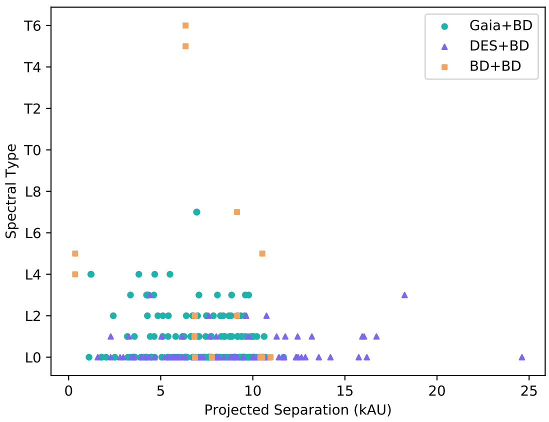

Figure 6. Spectral type of the brown dwarfs plotted against the projected separation of the pair. The green dots and the purple triangles represent the brown dwarf companions of Gaia DR2 and DES stars, respectively. The orange boxes indicate the systems composed by two brown dwarfs.

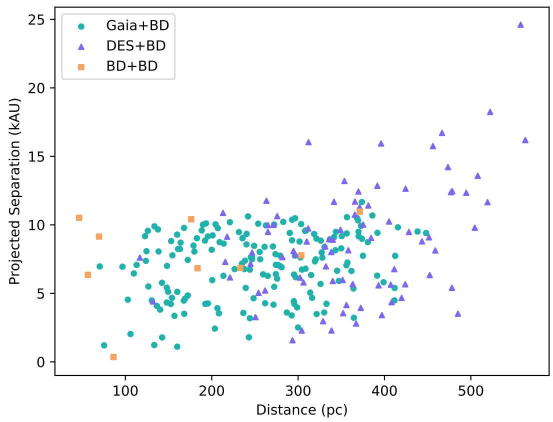

Figure 7. Projected pair separation in kAU plotted against distance for the 264 binary candidates with $P_a < 5$ %. The colours and different symbols represent the three different samples presented previously, as indicated in the upper left corner. The zone of avoidance at small projected separations (< 1 kAU) is caused by spatial resolution limits, while the scarcity of pairs with separations larger than 10,000 AU, specially for distances smaller than $\simeq 300$ pc, is due to the search method.

We also perform a search using the catalogue presented in Dhital et al. (2011) and Dhital et al. (2015), which contains low mass stars wide binaries identified using common distance and/or common proper motion. In this case, we

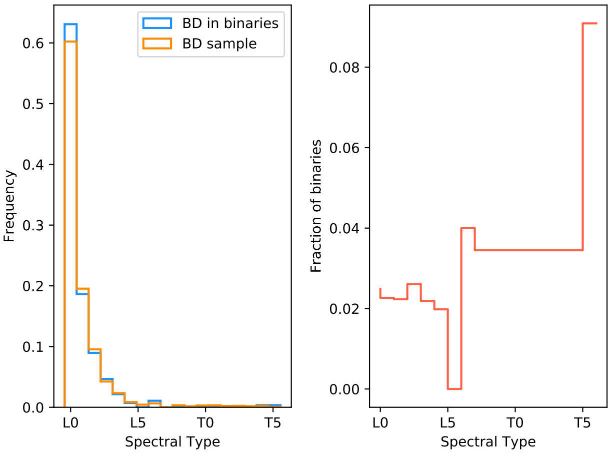

Figure 8. The left panel shows the total frequency distribution of L and T dwarfs (blue line) and of brown dwarfs in candidate wide binary systems (orange line), both as a function of spectral type. The right panel shows the observed fraction of wide binaries (in the separation range as shown in Figure 7) as a function of spectral type.

were able to identify one common system. In Dhital et al. (2015) the system is presented as an M1+M1 binary pair, but we identified as the quadruple system (J0239−0512) described in Section 5.3.

8 SUMMARY AND CONCLUSIONS

Using the Gaia DR2 and the combination of DES, VHS and AllWISE data along with a sample of L and T candidates from Carnero Rosell et al. (2019), we identified 264 new wide binary candidates containing a L or T dwarf. The projected separations for the wide binary pairs are spread within the ~ 600-10,000 AU range. A sample of six multiple systems were also identified and the projected separations between the brown dwarfs and the stellar members of these higher order systems range from ~ 3,000-11,000 AU.

Our candidates were selected based on common distance criteria and with a chance alignment probability criterion of $P_a < 5\%$. These binary and multiple system candidates involving substellar sources are crucial as benchmarks to evolutionary models below the hydrogen burning limit since properties such as metallicity and age, as well as masses, may be obtained for the primaries. The upper limit in projected distance results from our search strategy, in which we avoided larger separations that are more likely to be affected by contaminants. The lower limit in separation stems from the typical resolution of the DES images on which the brown dwarf sample is based.

We found 174 pairs with a primary from the Gaia DR2 catalogue limited to $G < 18$, for which distances are estimated from the `StarHorse` code using constraints from their measured parallaxes. We also found 81 pairs with a primary from the DES DR1 sample. These latter tend to be fainter and their `StarHorse` distances are based mostly on photometry, although some have Gaia DR2 parallax information as well. In addition, we found nine systems containing two

Table 4. Summary of the systems found. The systems with chance alignment probability >5% are not included here.

Type of system		Total
	Gaia+BD	174
Binary	DES+BD	81
	BD+BD	9
Triple		5
Quadruple		1

brown dwarfs. We found in total 264 new wide binary candidates. This is the largest sample of wide binary systems to date.

We also found six multiple systems, of which five are triples and one is a quadruple. The only potential quadruple system found is composed of an L0 dwarf associated to a star and to an M1+M1 double found previously by Dhital et al. (2015). One of the five triples is composed by two brown dwarfs associated with a DES star companion.

Table 4 summarizes all the systems found in this work, regarding its type and the total number of systems. About 64% of our brown dwarfs found in binary and multiple systems are of the L0 spectral type. Still they make up only $\simeq$ 2% of the total sample of L0 by Carnero Rosell et al. (2019). The typical wide binary fraction for the binary candidates over all spectral types ranges from 2 − 4% in the projected separation range covered by this work. The wide binary systems with L and T dwarfs as members presented here comprehend the largest catalogue to date. Despite the measurements of the chance alignment probabilities, unrelated systems could still be present in our sample. However, this catalogue constitutes a significant leap in the number of wide benchmark systems and in the estimates of the wide binary fraction involving substellar companions. A detailed investigation of these benchmark systems will provide constraints for the formation and evolution models as well as atmosphere models.

ACKNOWLEDGMENTS

Funding for the DES Projects has been provided by the U.S. Department of Energy, the U.S. National Science Foundation, the Ministry of Science and Education of Spain, the Science and Technology Facilities Council of the United Kingdom, the Higher Education Funding Council for England, the National Center for Supercomputing Applications at the University of Illinois at Urbana-Champaign, the Kavli Institute of Cosmological Physics at the University of Chicago, the Center for Cosmology and Astro-Particle Physics at the Ohio State University, the Mitchell Institute for Fundamental Physics and Astronomy at Texas A&M University, Financiadora de Estudos e Projetos, Fundação Carlos Chagas Filho de Amparo à Pesquisa do Estado do Rio de Janeiro, Conselho Nacional de Desenvolvimento Científico e Tecnológico and the Ministério da Ciência, Tecnologia e Inovação, the Deutsche Forschungsgemeinschaft and the Collaborating Institutions in the Dark Energy Survey.

The Collaborating Institutions are Argonne National Laboratory, the University of California at Santa Cruz, the University of Cambridge, Centro de Investigaciones

Energéticas, Medioambientales y Tecnológicas-Madrid, the University of Chicago, University College London, the DES-Brazil Consortium, the University of Edinburgh, the Eidgenössische Technische Hochschule (ETH) Zürich, Fermi National Accelerator Laboratory, the University of Illinois at Urbana-Champaign, the Institut de Ciències de l'Espai (IEEC/CSIC), the Institut de Física d'Altes Energies, Lawrence Berkeley National Laboratory, the Ludwig-Maximilians Universität München and the associated Excellence Cluster Universe, the University of Michigan, the NSFâĂŹs National Optical-Infrared Astronomy Research Laboratory, the University of Nottingham, The Ohio State University, the University of Pennsylvania, the University of Portsmouth, SLAC National Accelerator Laboratory, Stanford University, the University of Sussex, Texas A&M University, and the OzDES Membership Consortium.

Based in part on observations at Cerro Tololo Inter-American Observatory, NSFâĂŹs National Optical-Infrared Astronomy Research Laboratory, which is operated by the Association of Universities for Research in Astronomy (AURA) under a cooperative agreement with the National Science Foundation.

The DES data management system is supported by the National Science Foundation under Grant Numbers AST-1138766 and AST-1536171. The DES participants from Spanish institutions are partially supported by MINECO under grants AYA2015-71825, ESP2015-66861, FPA2015-68048, SEV-2016-0588, SEV-2016-0597, and MDM-2015-0509, some of which include ERDF funds from the European Union. IFAE is partially funded by the CERCA program of the Generalitat de Catalunya. Research leading to these results has received funding from the European Research Council under the European Union's Seventh Framework Program (FP7/2007-2013) including ERC grant agreements 240672, 291329, and 306478. We acknowledge support from the Australian Research Council Centre of Excellence for All-sky Astrophysics (CAASTRO), through project number CE110001020, and the Brazilian Instituto Nacional de Ciência e Tecnologia (INCT) e-Universe (CNPq grant 465376/2014-2).

This manuscript has been authored by Fermi Research Alliance, LLC under Contract No. DE-AC02-07CH11359 with the U.S. Department of Energy, Office of Science, Office of High Energy Physics. The United States Government retains and the publisher, by accepting the article for publication, acknowledges that the United States Government retains a non-exclusive, paid-up, irrevocable, world-wide license to publish or reproduce the published form of this manuscript, or allow others to do so, for United States Government purposes.

This publication makes use of data products from the Wide-field Infrared Survey Explorer, which is a joint project of the University of California, Los Angeles, and the Jet Propulsion Laboratory/California Institute of Technology, and NEOWISE, which is a project of the Jet Propulsion Laboratory/California Institute of Technology. WISE and NEOWISE are funded by the National Aeronautics and Space Administration.

The analysis presented here is based on observations obtained as part of the VISTA Hemisphere Survey, ESO Programme, 179.A-2010 (PI: McMahon).

This paper has gone through internal review by the DES collaboration.

ACR acknowledges financial support provided by the PAPDRJ CAPES/FAPERJ Fellowship and by "Unidad de Excelencia María de Maeztu de CIEMAT - Física de Partículas (Proyecto MDM)".

REFERENCES

Abazajian K. N., et al., 2009, ApJS, 182, 543
Abbott T. M. C., et al., 2018, ApJS, 239, 18
Anders F., et al., 2019, A&A, 628, A94
Anderson E., Francis C., 2012, Astronomy Letters, 38, 331
Arnouts S., Cristiani S., Moscardini L., Matarrese S., Lucchin F., Fontana A., Giallongo E., 1999, MNRAS, 310, 540
Bailey V., et al., 2014, ApJ, 780, L4
Baron F., et al., 2015, ApJ, 802, 37
Bate M. R., Bonnell I. A., 2005, MNRAS, 356, 1201
Bechtol K., et al., 2015, ApJ, 807, 50
Billères M., Delfosse X., Beuzit J.-L., Forveille T., Marchal L., Martín E. L., 2005, A&A, 440, L55
Bonnell I. A., Clark P., Bate M. R., 2008, MNRAS, 389, 1556
Bouy H., Brandner W., Martín E. L., Delfosse X., Allard F., Basri G., 2003, AJ, 126, 1526
Bowler B. P., Liu M. C., Cushing M. C., 2009, ApJ, 706, 1114
Bowler B. P., Liu M. C., Shkolnik E. L., Tamura M., 2012, ApJ, 756, 69
Bressan A., Marigo P., Girardi L., Salasnich B., Dal Cero C., Rubele S., Nanni A., 2012, MNRAS, 427, 127
Burgasser A. J., et al., 2000, ApJ, 531, L57
Burgasser A. J., Reid I. N., Leggett S. K., Kirkpatrick J. D., Liebert J., Burrows A., 2005, ApJ, 634, L177
Burgasser A. J., Luk C., Dhital S., Bardalez Gagliuffi D., Nicholls C. P., Prato L., West A. A., Lépine S., 2012, ApJ, 757, 110
Burningham B., et al., 2009, MNRAS, 395, 1237
Burningham B., et al., 2010, MNRAS, 404, 1952
Burningham B., et al., 2013, Monthly Notices of the Royal Astronomical Society, 433, 457
Caballero J. A., 2007, ApJ, 667, 520
Carlstrom J. E., et al., 2011, PASP, 123, 568
Carnero Rosell A., et al., 2019, arXiv e-prints, p. arXiv:1903.10806
Casagrande L., Schönrich R., Asplund M., Cassisi S., Ramírez I., Meléndez J., Bensby T., Feltzing S., 2011, A&A, 530, A138
Chabrier G., 2003, Publications of the Astronomical Society of the Pacific, 115, 763
Chauvin G., et al., 2005, A&A, 438, L29
Close L. M., Siegler N., Freed M., Biller B., 2003, ApJ, 587, 407
Cruz K. L., et al., 2007, AJ, 133, 439
Currie T., Burrows A., Daemgen S., 2014, ApJ, 787, 104
Day-Jones A. C., et al., 2011, MNRAS, 410, 705
De Rosa R. J., et al., 2015, ApJ, 814, L3
Deacon N. R., et al., 2012a, ApJ, 755, 94
Deacon N. R., et al., 2012b, ApJ, 757, 100
Deacon N. R., et al., 2014, ApJ, 792, 119
Deacon N. R., Schlieder J. E., Murphy S. J., 2016, MNRAS, 457, 3191
Deacon N. R., et al., 2017, MNRAS, 467, 1126
Desrochers M.-E., Artigau É., Gagné J., Doyon R., Malo L., Faherty J. K., Lafrenière D., 2018, ApJ, 852, 55
Dhital S., Burgasser A. J., Looper D. L., Stassun K. G., 2011, AJ, 141, 7
Dhital S., West A. A., Stassun K. G., Schluns K. J., Massey A. P., 2015, AJ, 150, 57
Drlica-Wagner A., et al., 2015, ApJ, 813, 109
Dupuy T. J., Liu M. C., 2012, Apjs, 201, 19
Dupuy T. J., et al., 2018, AJ, 156, 57

Elmegreen B. G., 2011, ApJ, 731, 61
Epchtein N., et al., 1997, The Messenger, 87, 27
Faherty J. K., Burgasser A. J., West A. A., Bochanski J. J., Cruz K. L., Shara M. M., Walter F. M., 2010, AJ, 139, 176
Faherty J. K., Burgasser A. J., Bochanski J. J., Looper D. L., West A. A., van der Bliek N. S., 2011, AJ, 141, 71
Flaugher B., et al., 2015, AJ, 150, 150
Forveille T., et al., 2004, A&A, 427, L1
Gaia Collaboration Brown A. G. A., Vallenari A., Prusti T., de Bruijne J. H. J., Babusiaux C., Bailer-Jones C. A. L., 2018, preprint, (arXiv:1804.09365)
Gálvez-Ortiz M. C., Solano E., Lodieu N., Aberasturi M., 2017, MNRAS, 466, 2983
Gauza B., Béjar V. J. S., Pérez-Garrido A., Rosa Zapatero Osorio M., Lodieu N., Rebolo R., Pallé E., Nowak G., 2015, ApJ, 804, 96
Girardi L., Groenewegen M. A. T., Hatziminaoglou E., da Costa L., 2005, A&A, 436, 895
Gizis J. E., Monet D. G., Reid I. N., Kirkpatrick J. D., Burgasser A. J., 2000, MNRAS, 311, 385
Gizis J. E., Kirkpatrick J. D., Wilson J. C., 2001, AJ, 121, 2185
Goldman B., Marsat S., Henning T., Clemens C., Greiner J., 2010, MNRAS, 405, 1140
Golimowski D. A., et al., 2004, AJ, 128, 1733
Gomes J. I., et al., 2013, MNRAS, 431, 2745
Ilbert O., et al., 2006, A&A, 457, 841
Kaiser N., et al., 2010, in Proc. SPIE. p. 77330E, doi:10.1117/12.859188
Kirkpatrick J. D., et al., 2000, AJ, 120, 447
Kirkpatrick J. D., et al., 2011, The Astrophysical Journal Supplement Series, 197, 19
Kraus A. L., Ireland M. J., Cieza L. A., Hinkley S., Dupuy T. J., Bowler B. P., Liu M. C., 2014, ApJ, 781, 20
Lafrenière D., Jayawardhana R., van Kerkwijk M. H., 2008, ApJ, 689, L153
Lawrence A., et al., 2007, Monthly Notices of the Royal Astronomical Society, 379, 1599
Loutrel N. P., Luhman K. L., Lowrance P. J., Bochanski J. J., 2011, ApJ, 739, 81
Luhman K. L., et al., 2007, ApJ, 654, 570
Luhman K. L., Burgasser A. J., Bochanski J. J., 2011, ApJ, 730, L9
Luhman K. L., et al., 2012, ApJ, 760, 152
Luque E., et al., 2017, MNRAS, 468, 97
Mace G. N., et al., 2013, ApJ, 777, 36
Marocco F., et al., 2017, MNRAS, 470, 4885
Martin E. L., Brandner W., Basri G., 1999, Science, 283, 1718
McCaughrean M. J., Close L. M., Scholz R. D., Lenzen R., Biller B., Brandner W., Hartung M., Lodieu N., 2004, A&A, 413, 1029
McMahon R. G., Banerji M., Gonzalez E., Koposov S. E., Bejar V. J., Lodieu N., Rebolo R., VHS Collaboration 2013, The Messenger, 154, 35
Metchev S. A., Hillenbrand L. A., 2004, ApJ, 617, 1330
Metchev S. A., Hillenbrand L. A., 2006, ApJ, 651, 1166
Mugrauer M., Seifahrt A., Neuhäuser R., Mazeh T., 2006, MNRAS, 373, L31
Mugrauer M., Neuhäuser R., Mazeh T., 2007, A&A, 469, 755
Murray D. N., et al., 2011, MNRAS, 414, 575
Mužić K., et al., 2012, AJ, 144, 180
Naud M.-E., et al., 2014, ApJ, 787, 5
Neuhäuser R., Guenther E. W., Wuchterl G., Mugrauer M., Bedalov A., Hauschildt P. H., 2005, A&A, 435, L13
Phan-Bao N., et al., 2008, MNRAS, 383, 831
Pinfield D. J., et al., 2012, MNRAS, 422, 1922
Queiroz A. B. A., et al., 2018, MNRAS, 476, 2556
Radigan J., Lafrenière D., Jayawardhana R., Doyon R., 2008, ApJ, 689, 471
Raghavan D., et al., 2010, ApJS, 190, 1
Rebolo R., Zapatero Osorio M. R., Madruga S., Bejar V. J. S., Arribas S., Licandro J., 1998, Science, 282, 1309
Reid I. N., Walkowicz L. M., 2006, Publications of the Astronomical Society of the Pacific, 118, 671
Reylé C., et al., 2013, Memorie della Societa Astronomica Italiana, 84, 1050
Scholz R. D., 2010a, A&A, 510, L8
Scholz R. D., 2010b, A&A, 515, A92
Scholz R.-D., 2016, A&A, 587, A51
Scholz R. D., McCaughrean M. J., Lodieu N., Kuhlbrodt B., 2003, A&A, 398, L29
Seifahrt A., Guenther E., Neuhäuser R., 2005, A&A, 440, 967
Skrutskie M. F., et al., 2006, AJ, 131, 1163
Skrzypek N., Warren S. J., Faherty J. K., Mortlock D. J., Burgasser A. J., Hewett P. C., 2015, A&A, 574, A78
Skrzypek N., Warren S. J., Faherty J. K., 2016, A&A, 589, A49
Smart R. L., Marocco F., Caballero J. A., Jones H. R. A., Barrado D., Beamín J. C., Pinfield D. J., Sarro L. M., 2017, MNRAS, 469, 401
Smith L. C., et al., 2015, MNRAS, 454, 4476
Sorahana S., Nakajima T., Matsuoka Y., 2018, preprint, (arXiv:1811.07496)
Tokovinin A., Lépine S., 2012, AJ, 144, 102
Whitworth A. P., Zinnecker H., 2004, A&A, 427, 299
Wilson J. C., Kirkpatrick J. D., Gizis J. E., Skrutskie M. F., Monet D. G., Houck J. R., 2001, AJ, 122, 1989
Wright E. L., et al., 2010, AJ, 140, 1868
York D. G., et al., 2000, AJ, 120, 1579
Zhang Z., 2019, MNRAS, 489, 1423
Zhang Z. H., et al., 2010, MNRAS, 404, 1817

9 AFFILIATIONS

[1] Instituto de Física, UFRGS, Caixa Postal 15051, Porto Alegre, RS - 91501-970, Brazil
[2] Laboratório Interinstitucional de e-Astronomia - LIneA, Rua Gal. José Cristino 77, Rio de Janeiro, RJ - 20921-400, Brazil
[3] Centro de Investigaciones Energéticas, Medioambientales y Tecnológicas (CIEMAT), Madrid, Spain
[4] Center for Astrophysics Research, University of Hertfordshire, Hatfield AL10 9AB, UK
[5] Fermi National Accelerator Laboratory, P. O. Box 500, Batavia, IL 60510, USA
[6] George P. and Cynthia Woods Mitchell Institute for Fundamental Physics and Astronomy, and Department of Physics and Astronomy, Texas A&M University, College Station, TX 77843, USA
[7] LSST, 933 North Cherry Avenue, Tucson, AZ 85721, USA
[8] Physics Department, 2320 Chamberlin Hall, University of Wisconsin-Madison, 1150 University Avenue Madison, WI
[9] Center for Cosmology and Astro-Particle Physics, The Ohio State University, Columbus, OH 43210, USA
[10] Department of Astronomy, The Ohio State University, Columbus, OH 43210, USA
[11] Department of Astrophysical Sciences, Princeton University, Peyton Hall, Princeton, NJ 08544, USA
[12] Kavli Institute for Cosmological Physics, University of Chicago, Chicago, IL 60637, USA
[13] Observatories of the Carnegie Institution for Science, 813 Santa Barbara St., Pasadena, CA 91101, USA
[14] Cerro Tololo Inter-American Observatory, NSFâĂŹs National Optical-Infrared Astronomy Research Laboratory,

Casilla 603, La Serena, Chile
[15] Departamento de Física Matemática, Instituto de Física, Universidade de São Paulo, CP 66318, São Paulo, SP, 05314-970, Brazil
[16] Instituto de Fisica Teorica UAM/CSIC, Universidad Autonoma de Madrid, 28049 Madrid, Spain
[17] CNRS, UMR 7095, Institut d'Astrophysique de Paris, F-75014, Paris, France
[18] Sorbonne Universités, UPMC Univ Paris 06, UMR 7095, Institut d'Astrophysique de Paris, F-75014, Paris, France
[19] Department of Physics and Astronomy, Pevensey Building, University of Sussex, Brighton, BN1 9QH, UK
[20] Department of Physics & Astronomy, University College London, Gower Street, London, WC1E 6BT, UK
[21] Department of Astronomy, University of Illinois at Urbana-Champaign, 1002 W. Green Street, Urbana, IL 61801, USA
[22] National Center for Supercomputing Applications, 1205 West Clark St., Urbana, IL 61801, USA
[23] Institut de Física d'Altes Energies (IFAE), The Barcelona Institute of Science and Technology, Campus UAB, 08193 Bellaterra (Barcelona) Spain
[24] Observatório Nacional, Rua Gal. José Cristino 77, Rio de Janeiro, RJ - 20921-400, Brazil
[25] Department of Astronomy/Steward Observatory, University of Arizona, 933 North Cherry Avenue, Tucson, AZ 85721-0065, USA
[26] Jet Propulsion Laboratory, California Institute of Technology, 4800 Oak Grove Dr., Pasadena, CA 91109, USA
[27] Santa Cruz Institute for Particle Physics, Santa Cruz, CA 95064, USA
[28] Institut d'Estudis Espacials de Catalunya (IEEC), 08034 Barcelona, Spain
[29] Institute of Space Sciences (ICE, CSIC), Campus UAB, Carrer de Can Magrans, s/n, 08193 Barcelona, Spain
[30] Department of Astronomy, University of Michigan, Ann Arbor, MI 48109, USA
[31] Department of Physics, University of Michigan, Ann Arbor, MI 48109, USA
[32] Department of Physics, Stanford University, 382 Via Pueblo Mall, Stanford, CA 94305, USA
[33] SLAC National Accelerator Laboratory, Menlo Park, CA 94025, USA
[34] School of Mathematics and Physics, University of Queensland, Brisbane, QLD 4072, Australia
[35] Department of Physics, The Ohio State University, Columbus, OH 43210, USA
[36] Center for Astrophysics | Harvard & Smithsonian, 60 Garden Street, Cambridge, MA 02138, USA
[37] Australian Astronomical Optics, Macquarie University, North Ryde, NSW 2113, Australia
[38] Lowell Observatory, 1400 Mars Hill Rd, Flagstaff, AZ 86001, USA
[39] Department of Physics and Astronomy, University of Pennsylvania, Philadelphia, PA 19104, USA
[40] Institució Catalana de Recerca i Estudis Avançats, E-08010 Barcelona, Spain
[41] School of Physics and Astronomy, University of Southampton, Southampton, SO17 1BJ, UK
[42] Computer Science and Mathematics Division, Oak Ridge National Laboratory, Oak Ridge, TN 37831
[43] Institute of Cosmology and Gravitation, University of Portsmouth, Portsmouth, PO1 3FX, UK
[44] Max Planck Institute for Extraterrestrial Physics, Giessenbachstrasse, 85748 Garching, Germany
[45] Universit"ats-Sternwarte, Fakult"at f"ur Physik, Ludwig-Maximilians Universit"at M"unchen, Scheinerstr. 1, 81679 M"unchen, Germany

APPENDIX A: TABLES FROM THE LITERATURE

Table A1: Known binaries which contain a brown dwarfs as a secondary, all are spectroscopically confirmed. All the systems presented here have projected separation > 100 AU. This table was based on Table 12 from Deacon et al. (2014).

Object	Separation		Spectral Type		Mass	Age	References
ID	"	AU	Companion	Primary	$M_{\odot}$	Gyr	
HD65216BC	7.00	253	M7+L2	G5	0.08	3-6	1
LP213-68Bab	14.00	230	M8+L1	M6.5	0.068-0.090	-	14,15
BD+131727B	10.5	380	M8+L0.5	K5	-	-	13
HD221356BC	452.00	11900	M8+L3	F8	0.072	5.5-8	27
HD221356D	12.13	2050	L1	F8+M8+L3	0.073-0.085	2.5-7.9	32
DENISJ0551-4434B	2.20	220	L0	M8.5	0.06	0.1-10	5
Denis-PJ1347-7610B	16.80	418	L0	M0	-	0.2-1.4	6
HD89744B	63.00	2460	L0	F7	0.077-0.080	1.5-3	7
NLTT2274B	23.00	483	L0	M4	0.081-0.083	4.5-10.0	8
LP312-49B	15.40	801	L0	M4	-	-	9
SDSSJ130432.93+090713.7B	7.60	374	L0	M4.5	-	-	9
SDSSJ163814.32+321133.5B	46.00	2420	L0	M4	-	-	9
1RXSJ235133.3+312720B	2.40	120	L0	M2	0.026-0.038	0.05-0.15	10
2MASS12593933+0651255	23.86	1110	L0	M8	0.21	0.5	11
2MASS09411195+3315060	7.44	244	L0	M5	0.23	<10	11
HIP2397B	117.1	3970	L0.5	K5	-	0.5-10	12
HD253662B	20.1	>1252	L0.5	G8	-	<10	12
2M0858+2710	15.6	780	L0	M4	0.074-0.081	-	28
2M1021+3704	22.2	3000	L0	M4	0.071-0.076	-	28
2M0013-1816	118.1	7400	L1	M3	0.072-0.078	-	28
2M1202+4204	7.3	310	L0	M6	0.074-0.081	-	28
2M0005+0626	6.1	400	L0	M4.5	0.079-0.085	-	28
GaiaJ0452-36A	115.3	15828	L0	M1	0.084-0.086	-	29
2M1441+1856	51.1	4110	L1	M6	0.072-0.079	-	28
HIP59933B	38.10	2170	L1	F8	-	0.3-2.5	12
HIP63506B	132.8	5640	L1	M0	-	0.3-10	12
HIP6407B	44.90	2570	L1+T3	G5	-	0.5-10	12
GJ1048B	11.90	250	L1	K2	0.055-0.075	0.6-2	16
ABPicB	5.50	275	L1	K2	0.01	0.03	17
G124-62Bab	44.00	1496	L1+L1	dM4.5e	0.054-0.082	0.5-0.8	18
HD16270	11.90	254	L1	K3.5	-	0.0015-0.003	2,16,4
GQLupB	0.70	103	L1	K7	0.010-0.020	<0.002	19
ROX42Bb	1.80	140	L1	M1	0.006-0.014	0.0015-0.003	20,21
LSPMJ0241+2553B	31.20	2153	L1	WD	-	<10	12
HIP112422B	16.0	1040	L1.5	K2	-	0.1-10	12
LSPMJ0632+5053B	47.4	4499	L1.5	G2	-	0.2-10	12
PMI13518+4157B	21.6	613	L1.5	M2.5	-	0.3-10	12
NLTT44368B	90.2	7760	L1.5	M3	-	0.3-10	12
PM122118-1005B	204.5	8892	L1.5	M2	-	0.3-10	12
β Cir	217.8	6656	L1	A3V	0.056	0.2-10.0	22
2M0122+0331	44.8	2222	L2	G5	0.071-0.076	-	28
NLTT1011B	58.5	3990	L2	K7	-	0.3-10.0	12
G255-34B	38.30	1364	L2	K8	-	-	23
2MASSJ05254550-7425263B	44.00	2000	L2	M3	0.06-0.075	1.0-10	24
G196-3B	16.20	300	L2	M2.5	0.015-0.04	0.06-0.3	25
Gl618.1B	35.00	1090	L2.5	M0	0.06-0.079	0.5-12	7
HD106906b	7.10	650	L2.5	F5	0.003-0.007	0.013-0.015	26
2MASSJ0249-0557AB	39.9	1950	L2	M6	0.010-0.012	0.016-0.028	39
G63-33B	66.00	2010	L3	K2	0.079-0.081	3.3-5.1	8
G73-26B	73.00	2774	L3	M2	0.079-0.081	3.0-4.0	8,9
2MASSJ2126-8140	217	6900	L3	M2	0.014-0.011	0.01-0.150	49
2MASSJ22501512+2325342	8.9	518	L3	M3	-	0.015	50
ηCancriB	164.00	15020	L3.5	K3III	0.063-0.082	2.2-6.1	9
NLTT26746B	18.0	661	L4	M4	-	0.3-10	12
PMI13410+0542B	9.4	484	L4	M1	-	0.3-10	12

Table A1 – **continued from previous page**

Object ID	Separation ”	AU	Spectral Type Companion	Primary	Mass $M_{\odot}$	Age Gyr	References
G171-58B	218.00	9200	L4	F8	0.045-0.083	1.8-3.5	8
G200-28B	570.00	25700	L4	G5	0.077-0.078	7.0-12.0	8
LHS5166B	8.43	160	L4	M4.5	0.055-0.075	2.6-8	18
1RXSJ1609-2105b	2.20	330	L4	M0	0.009-0.016	0.010-0.013	33
2M1259+1001	7.65	345	L4.5	M5	0.057-0.074	-	28
GJ1001Bc	18.60	180	L4.5+L4.5	M4	0.060-0.075	1-10	29,34,35
Gl417Bab	90.00	2000	L4.5+L6	G0+G0	0.02-0.05	0.08-0.3	29,36
2M1115+1607	18.1	660	L5	M4	0.056-0.073	-	28
G203-50B	6.40	135	L5.0	M4.5	0.051-0.074	1-5	37
GJ499C	516.00	9708	L5	K5+M4	-	-	23
G259-20B	30.00	650	L5	M2.5	-	-	38
HD 196180	13.51	907	L5	A3V	-	0.3	40
NLTT55219B	9.7	432	L5.5	M2	-	0.1-0.2	12
NLTT31450B	12.30	487	L6	M4	-	0.3-10	12
LP261-75B	13.00	450	L6	M4.5	0.019-0.025	0.1-0.2	41
2MASSJ01303563-4445411B	3.28	130	L6	M9	0.032-0.076	0.25-0.8	42
NLTT 20346	248	7700	L7+L6.5	M5+M6	0.070	-	47
VHS1256-1257	8.06	102	L7	M7.5	0.010	0.015-0.030	43
HD203030B	11.00	487	L7.5	G8	0.012-0.031	0.13-0.4	44
Gl337CD	43.00	880	L8+L8	G8+K1	0.04-0.074	0.6-3.4	7,45
Gl584C	194.00	3600	L8	G1	0.045-0.075	1-2.5	46
HD46588B	79.20	1420	L9	F7	0.045-0.072	1.3-4.3	48
ϵ IndiBab	402.00	1460	T1	K5	0.06-0.073	~5	53,54
2MASSJ111806.99-064007.8B	7.70	650	T2	M4.5	0.06-0.07	-	55
HNPegB	43.00	795	T2.5	G0	0.012-0.030	0.1-0.5	56
2MASSJ0213+3648ABC	16.4	360	T3	M4.5+M6.5	0.068	1	51
GUPscB	41.97	2000	T3.5	M3	0.07-0.13	0.009-0.0013	57
HIP38939B	88.00	1630	T4.5	K4	0.018-0.058	0.3-2.8	58
LSPMJ1459+0851B	365.00	21500	T4.5	DA	0.064-0.075	4-10	59
SDSSJ0006-0852AB		820	T5	M7+M8.5	0.056	-	52
LHS2803B	67.60	1400	T5	M4.5	0.068-0.081	3.5-10	24,60
HD118865B	148.00	9200	T5	F5	-	1.5-4.9	61
HIP73786B	63.80	1230	T6	K5	-	>1.6	62,63
LHS302B	265.00	4500	T6	M5	-	-	64
G204-39B	198.00	2685	T6.5	M3	0.02-0.035	0.5-3.0	8
Gl570D	258.00	1500	T7	K4+M2+M3	0.03-0.07	2-5	65
HD3651B	43.00	480	T7.5	K0	0.018-0.058	0.7-4.7	56,66
SDSSJ1416+30B	9.00	45-135	T7.5	L6	0.03-0.04	~10	67,68,69
LHS2907B	156.00	2680	T8	G1	0.019-0.047	2.3-14.4	38,70
LHS6176B	52.00	1400	T8	M4	-	>3.5	38,61
Wolf1130B	188.50	3000	T8	sdM1.5+DA	0.020-0.050	>2	71
Ross458C	102.00	1162	T8.5	M0.5+M7	0.005-0.0014	<1.0	72
ξ UMaE	510.00	4100	T8.5	F9+G0	0.014-0.038	4.0-8.0	61
Wolf940B	32.00	400	T8.5	M4	0.02-0.032	3.5-6	73
WD0806-661	130.00	2500	>Y0	DQ	0.03-0.10	1.2-2	74

Table A1 – continued from previous page

Object	Separation		Spectral Type		Mass	Age	References
ID	”	AU	Companion	Primary	$M_\odot$	Gyr	

References: (1) Mugrauer et al. (2007); (2) Anderson & Francis (2012); (3) Forveille et al. (2004); (4) Dupuy & Liu (2012); (5) Billères et al. (2005); (6) Phan-Bao et al. (2008); (7) Wilson et al. (2001); (8) Faherty et al. (2010); (9) Zhang et al. (2010); (10) Bowler et al. (2012); (11) Gálvez-Ortiz et al. (2017); (12) Deacon et al. (2014); (13) Cruz et al. (2007); (14) Gizis et al. (2000); (15) Close et al. (2003); (16) Gizis et al. (2001); (17) Chauvin et al. (2005); (18) Seifahrt et al. (2005); (19) Neuhäuser et al. (2005); (20) Kraus et al. (2014); (21) Currie et al. (2014); (22) Smith et al. (2015); (23) Gomes et al. (2013); (24) Mužić et al. (2012); (25) Rebolo et al. (1998); (26) Bailey et al. (2014); (27) Caballero (2007); (28) Baron et al. (2015); (29) Zhang (2019); (30) Casagrande et al. (2011); (31) Metchev & Hillenbrand (2004); (32) Caballero (2007); (33) Lafrenière et al. (2008); (34) Golimowski et al. (2004); (35) Martin et al. (1999); (36) Bouy et al. (2003); (37) Radigan et al. (2008); (38) Luhman et al. (2012); (39) Dupuy et al. (2018); (40) De Rosa et al. (2015); (41) Reid & Walkowicz (2006); (42) Dhital et al. (2011); (43) Gauza et al. (2015); (44) Metchev & Hillenbrand (2006); (45) Burgasser et al. (2005); (46) Kirkpatrick et al. (2000); (47) Faherty et al. (2011); (48) Loutrel et al. (2011); (49) Deacon et al. (2016); (50) Desrochers et al. (2018); (51) Deacon et al. (2017); (52) Burgasser et al. (2012); (53) Scholz et al. (2003); (54) McCaughrean et al. (2004); (55) Reylé et al. (2013); (56) Luhman et al. (2007); (57) Naud et al. (2014); (58) Deacon et al. (2012a); (59) Day-Jones et al. (2011); (60) Deacon et al. (2012b); (61) Burningham et al. (2013); (62) Scholz (2010b); (63) Murray et al. (2011); (64) Kirkpatrick et al. (2011); (65) Burgasser et al. (2000); (66) Mugrauer et al. (2006); (67) Scholz (2010a) ; (68) Burningham et al. (2010); (69) Bowler et al. (2009); (70) Pinfield et al. (2012); (71) Mace et al. (2013); (72) Goldman et al. (2010); (73) Burningham et al. (2009); (74) Luhman et al. (2011).

Table A2. The common-distance and common-proper-motion wide binary pairs identified in the literature.

Object ID	Separation kAU	Distance pc	Sp. Type Companion	Sp. Type Primary	$\mu_\alpha \cos\delta$ (mas yr^-1)	μ_δ (mas yr^-1)	References
J0223-5815	400	49 ±10	L0	M5	134.0±10	5.0±19	1
J1214+3721	153	82 ±17	L0	-	-122.6 ±10.6	82.0 ±17	1
J0939+3412	156	62 ±10	L0	-	-107.1 ±10.4	-64.3 ±12.6	1
ULAS J0255+0532	29	140 ±26	L0	F5	28 ±30	40 ±30	2
ULAS J0900+2930	16	197 ±37	L0	M3.5	-13 ±10	-27.8 ±8.8	2
ULAS J1222+1407	6.7	70 ±13	L0	M4	-74 ±20	-34 ±20	2
J0626+0029	252	67 ±14	L0.5	-	84 ±15	-92 ±15	1
J1632+3505	2	37 ±8	L0.5	K0	91.6 ±9.7	-65.3 ±11.9	1
J2037-4216	270	51 ±10	L1	-	229 ±10	-391 ±10	1
ULAS J1217+1427	2.7	216 ±41	L1	F8V	-49 ±8.2	-19.7 ±8.5	2
ULAS J1330+0914	61	149 ±30	L2	G5	-83 ±37	10 ±37	2
HD 3861 B			L3.5	F8V	-121 ±14	-79 ±13	3
J0230-0225	145	33 ±8	L8	K1	-105 ±8	-62.8 ±8.2	1
J1244+1232	286	46 ±8	T4	-	-104.8 ±8.6	4.5 ±7.3	1
J0758+2225	157	27 ±6	T6.5	-	329 ±16.8	51.3 ±14.9	1
J1150+0949	211	60 ±27	T6.5	-	-107.6 ±17.1	-31.9 ±4.5	1
J0915+0531	178	33 ±6	T7	-	-95 ±5.5	-57.7 ±4.4	1

References: (1) Smart et al. (2017); (2) Marocco et al. (2017); (3) Scholz (2016).